Characterization of the Organic Ligand Shell of Semiconductor Quantum Dots by Fluorescence Quenching Experiments

Klaus Boldt, Sebastian Jander, Kathrin Hoppe, and Horst Weller*

Institute for Physical Chemistry, University of Hamburg, Grindelallee 177, 20146 Hamburg, Germany

ABSTRACT We present the characterization of the organic ligand shell of CdSe/$Cd_xZn_{1-x}S$/ZnS nanoparticles by means of fluorescence quenching experiments. Both electron scavengers and acceptors for resonance energy transfer were employed as probes. Different quenching behavior for short and long chain thiol ligands in water was found. It could be shown that poly(ethylene oxide) (PEO)-capping of the particles comprises a densely packed inner shell and a loosely packed outer shell in which ions and small molecules diffuse unhindered. A quantitative uptake of quencher molecules into the PEO shell was observed, through which the particle volume including the ligand sphere could be determined.

KEYWORDS: quantum dots · ligands · electron transfer · FRET · cysteine · poly(ethylene) glycol

Semiconductor nanoparticles or quantum dots (QDs) have been proposed as fluorescent labels for biological samples, both *in vitro* and *in vivo*, as long as efficient synthetic routes to high quality QDs have been available.[1−3] Their advantage over organic dyes are their broad absorption and narrow emission band, large absorption cross section, adjustable emission wavelength and high photostability. The usual route to highly luminescent, monodisperse QDs is the hot injection synthesis in high-boiling, organic solvents.[4−6] To further enhance the fluorescence quantum yield (QY), one or more shells of a higher bandgap material are epitaxially grown onto the QDs in order to reduce the overlap of the excited electron and hole wave functions inside the core particle with surface trap states.[7]

For biological application the hydrophobic particles have to be transferred into aqueous solution. This can be done by ligand exchange,[8−11] intercalating water-soluble molecules into the organic ligand shell[12] or encapsulating the particles into micelles.[13] A wide range of organic molecules containing one or more thiol groups have been used for ligand exchange, including mercaptopropionic acid, dihydrolipoic acid, mercaptoundecanoic acid, and conjugates of these molecules with a polymer chain.[14] Very small cysteine-capped CdSe/ZnS particles have been synthesized by Liu *et al.*, which exhibit quantum yields of 10−15% and show renal clearance below a hydrodynamic diameter of 5.5 nm.[15] Polymer conjugates with a longer chain length result in a larger hydrodynamic radius, better long-term stability of the QDs, and a higher photoluminescence (PL) quantum yield. Poly(ethylene oxide) (PEO) has been widely employed as a capping agent, because it does not interact strongly with proteins and other molecules in blood serum or cell media.[16] Recently, we have published the synthesis of a versatile tridentate polyethylene oxide ligand with thiol anchor groups ($PEO(SH)_3$), which is extremely facile to produce. The PL QY of this system was determined to be as high as 43% in water.[17]

Apart from the particle size the potential use of water-soluble nanoparticles depends on the permeability of the organic layer for small molecules and ions. Blocking the access from the medium to the particle surface can effectively suppress PL quenching and decreases possible toxic effects from dissolving cadmium or selenide ions from the inorganic particle.[18] A thorough knowledge of its internal structure is therefore desirable.

Fluorescence quenching caused by electron transfer (ET), which is based on a tunneling process over the distance of a few Å, and Förster resonance energy transfer (FRET) between donor and acceptor fluorophores have been widely used to characterize nanoscale systems.[19−22] Because of the distance dependency of FRET in the order of several nanometers the penomenon has been called

* Address correspondence to weller@chemie.uni-hamburg.de.

Received for review July 20, 2011 and accepted September 25, 2011.

Published online September 25, 2011
10.1021/nn202748v

a "molecular ruler".[23] The applicability of FRET on QDs with a finite volume is not self-evident, since the theory describes donors and acceptors as point dipoles. Baer and Rabani have shown that QDs acting as donors can be described as dipoles within the effective mass approximation, because the radiative decay of the exciton is quadrupole forbidden.[24] Treatment of QDs as point dipoles is adequate for dipole distances that are larger than the particle size.[25] Allan *et al*. could show that Förster's theory is correct for nanoscale, direct semiconductors within tight-binding calculations by introducing a screening factor, which takes into account the dielectric constants of the donor, acceptor, and the surrounding medium.[26] Despite these limitations FRET is commonly applied to nanoparticle systems as the best available theory.[27−30]

In this publication we present the characterization of CdSe/$Cd_xZn_{1-x}S$/ZnS particles capped with $PEO(SH)_3$ or cysteine by deliberate PL quenching due to electron transfer or FRET in aqueous solution.

RESULTS AND DISCUSSION

Characterization of the Quantum Dots. Two batches of CdSe/$Cd_xZn_{1-x}S$/ZnS particles of different sizes were synthesized following the protocol of Talapin *et al*.[7] and used for electron transfer and FRET experiments, respectively. The first sample had a particle diameter of 5.8 ± 0.6 nm, determined from TEM measurements (Figure 1A). The size has been achieved by a growth time of 60 min for the core particles and subsequent growth of two chalcogenide sulfide shells in order to enhance PL QY. The first absorption maximum of the core/shell/shell particles was observed at a wavelength of 570 nm, the PL maximum at 585 nm (Figure 1B).

For fluorescence quenching due to FRET smaller particles were employed, with which optimal spectral overlap was achieved with the absorption spectrum of the employed organic dye, BODIPY TR. Also, the PL spectra of donor and acceptor were clearly separated. The growth of these particles was stopped immediately after precursor injection, which resulted in a diameter of 4.9 ± 0.6 nm, an absorption maximum at 531 nm and a PL maximum at a wavelength of 546 nm after shell growth (Figure 1C−D). A nucleation of $Cd_xZn_{1-x}S$/ZnS and ZnS particles occurred during the shell synthesis, the fluorescence of which could be observed as a high energy shoulder in the emission spectrum.

Ligand exchange with cysteine and $PEO(SH)_3$ was performed according to the protocols of Liu *et al*.[10] and Thiry *et al*.,[17] respectively. No significant shift in the absorption spectra was observed, while the particles' PL QY decreased in accordance with the results reported in the respective publications to a QY of 11% for cysteine and 26% for $PEO(SH)_3$ ligands in water. Typically, particle concentrations in the order of 500 nM were employed in the experiments.

Electron Transfer with Cysteine-Capped QDs. Methyl viologen dichloride and iron(III) nitrate were used as electron scavengers, which quench the fluorescence by extracting the excited electron from the QDs.[31,32] The methyl viologen cation MV^{2+} forms a redox system with the radical cation MV^{+} with a reduction potential of $E° = -0.44$ V close to the conduction band edge of bulk CdSe.[33] Fe^{3+} is reduced to Fe^{2+} at a potential of $E° = 0.77$ V.[34]

Cysteine-capped particles exhibited static quenching with either of the two electron scavengers, where the formation of a fluorophor−quencher complex creates a nonfluorescent species and the ensemble of emitting particles is depleted. This mechanism does not change the fluorescence lifetime, but reduces the initial photon count at $t = 0$ ns in the TCSPC spectra proportionally to the PL intensity (see Supporting Information, Figure S1). The slope of the linear Stern−Volmer plot is the equilibrium constant K_s for the formation of the fluorophor−quencher complex.[32] K_s was determined to be 17600 ± 300 L mol^{-1} for Fe^{3+} and 54000 ± 900 L mol^{-1} for MV^{2+}. Methyl viologen proved to be the more efficient quencher. The fluorescence intensity decreased to 80% at a concentration of 4.7 μM MV^{2+} or 14 μM Fe^{3+}. To achieve a quenching efficiency of 50%, a MV^{2+} concentration of 16 μM or an Fe^{3+} concentration of 66 μM were necessary. No apparent dependency of the quenching behavior on the particle concentration was observed between 10 and 800 nmol.

The Stern−Volmer constant K_s was used to fit the normalized fluorescence intensity as a function of the quencher concentration [Q] with a Langmuir adsorption model (Figures 2 and 3).

$$(1 - \theta) = \frac{1}{1 + K_s[Q]} \qquad (1)$$

The fit reproduces the data very well for both Fe^{3+} and MV^{2+}. In the case of methyl viologen the adsorption behavior deviated from the Langmuir isotherm at high quencher concentrations. The onset of the deviation coincides with a kink in the Stern−Volmer plot, caused by the beginning of precipitation of QDs due to photooxidation of the ligands to disulfides. When other thiol ligands than cysteine (mercaptopropionic acid, dihydrolipoic acid, 1-thioglycerol) were employed, accelerated precipitation of the particles during the measurement occurred, which increased with increasing dilution and made an analysis of the data impossible.

Temperature dependent measurements in the range of 20−50 °C were performed for the quenching reaction with iron nitrate, which confirmed the Langmuir adsorption model. The van't Hoff plot of $\ln K_s$ against $1/T$ gave the thermodynamic parameters for the adsorption reaction (Figure 4). Measured values for the adsorption enthalpy, entropy, and Gibbs free enthalpy were $\Delta_R H° = -39.0 \pm 0.4$ kJ mol^{-1},

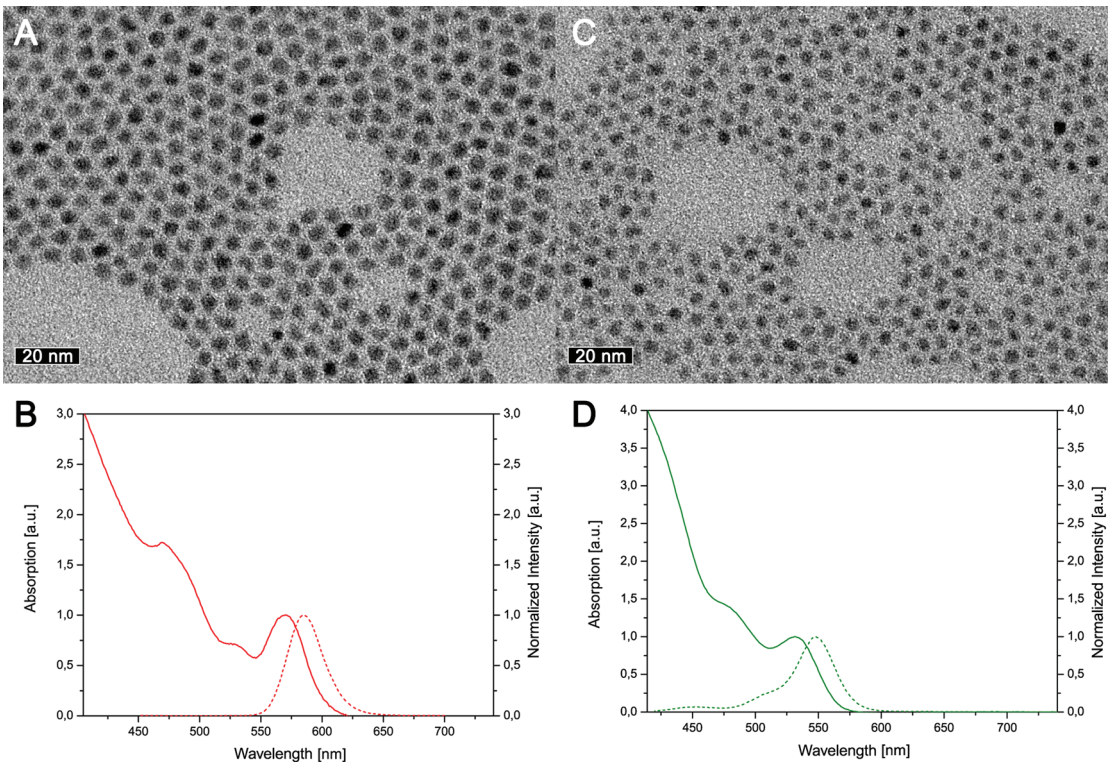

Figure 1. TEM images, absorption, and PL emission spectra of the 5.8 nm (A,B) and 4.9 nm-sized (B,C) core/shell/shell QDs in chloroform before ligand exchange.

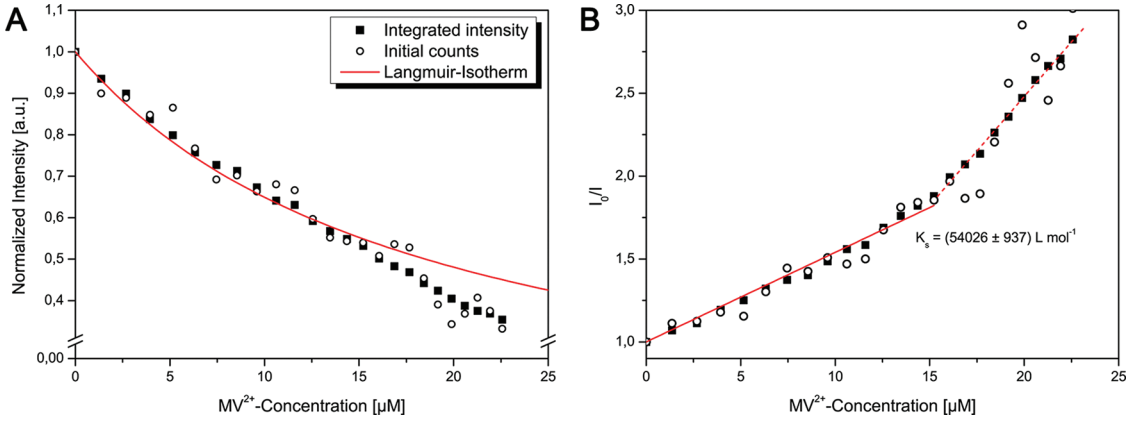

Figure 2. (A) Normalized, integrated fluorescence intensity (■) and initial counts of the fluorescence decay curve (○) of cysteine-capped QDs plotted against MV^{2+} concentration. (B) Stern–Volmer plot of the same data. Linear regression at lower MV^{2+} concentration yielded the Stern–Volmer constant K_s, which was used as a parameter for a Langmuir isotherm.

$\Delta_R S° = -38.2 \pm 0.02$ J mol^{-1} K^{-1} and $\Delta_R G° = -27.6 \pm 0.4$ kJ mol^{-1}. Adsorption of Fe^{3+} to cysteine-stabilized QDs is therefore enthalpy driven. Comparable values have been measured by Ding *et al.* for similar, cysteine-stabilized QDs with BSA as an adsorbate.[35] The free enthalpy corresponds to a physisorption reaction.

Electron Transfer with $PEO(SH)_3$-Capped QDs. Quenching of $PEO(SH)_3$-capped particles was found to follow a dynamic quenching mechanism, in contrast to particles stabilized with short, organic thiols. Dynamic quenching is explained by a diffusion-controlled electron transfer reaction, in which the transfer competes against the radiative decay and therefore reduces the fluorescence lifetime of the particles. Fe^{3+} ions quenched the PL to 80% of the original intensity at a concentration of 300 μM, which is a 4.5 times lower quenching efficiency in comparison to cysteine-capped QDs (Figure 5). The PL of single $PEO(SH)_3$-capped particles spin coated onto a glass cover slide was decreased in the presence of Fe^{3+} and dropped below the detection limit after 5–10 s of continuous irradiation (see Supporting Information). This irreversible bleaching happened on a larger time scale than

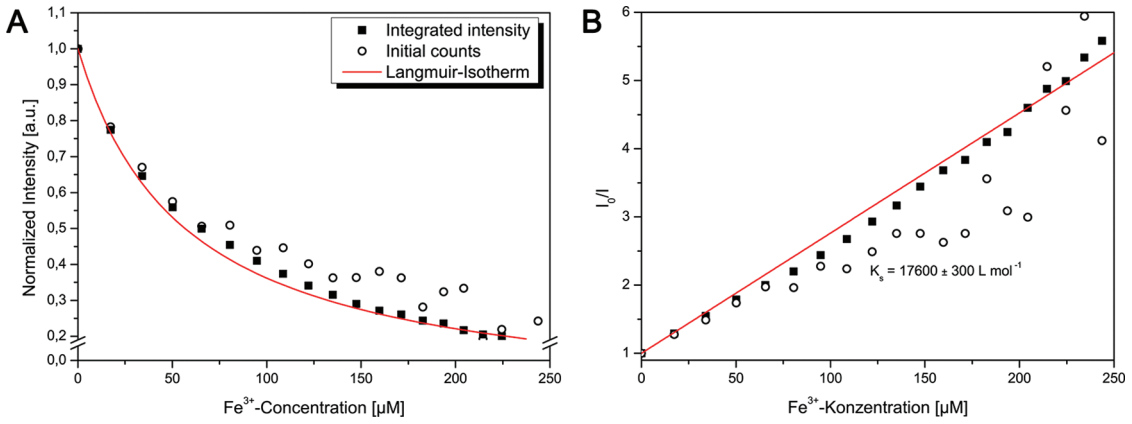

Figure 3. (A) Normalized, integrated fluorescence intensity (■) and initial counts of the fluorescence decay curve (○) of cysteine-capped QDs plotted against Fe^{3+} concentration. (B) Stern–Volmer plot of the same data. Linear regression yielded the Stern–Volmer constant K_s, which was used as a parameter for a Langmuir isotherm. Deviation of the initial counts from the total intensity at high quencher concentrations results from a small contribution of dynamic quenching.

both the electron transfer and particle diffusion through the excitation beam.

PEOs with a molar weight of 1000 and 2000 g mol^{-1} were used in the experiments and no dependency of the quenching efficiency on the polymer chain length was observed. This finding agrees with our earlier observations that the ligand number density on the particle surface decreases with an increasing PEO chain length due to the increasing volume of the coiled polymer.[17] The hydrodynamic diameter of the particles determined by dynamic light scattering (DLS) measurements varied between 20 and 30 nm. This correlates well with literature values for the hydrodynamic diameter of free PEO chains in water, which vary between 8 and 12.6 nm.[36]

The electron transfer rate constant k_{ET} can be calculated from the slope $K_d = \tau_0 k_{ET}$ for the Stern–Volmer plots of both PL intensity and fluorescence lifetime against the quencher concentration [Q].[32]

$$\frac{I_0}{I} = \frac{\tau_0}{\tau} = 1 + \tau_0 k_{ET}[Q] \qquad (2)$$

$\tau_0 = 13.6$ ns is the PL lifetime in the absence of electron scavengers. Assuming a diffusion controlled electron transfer reaction, the collision rate constant is equal to the rate of the quenching reaction and can be used to calculate the effective radius R_{QD} of the particles.

$$k_{ET} = 4\pi N_A f_Q (R_{QD} + R_{Fe^{3+}})(D_{QD} + D_{Fe^{3+}}) \qquad (3)$$

where N_A is Avogadro's number, f_Q is the quenching efficiency, and D is the diffusion coefficient for the specified components. Owing to the large size difference between the metal ion and the nanoparticle, the ion radius and particle diffusion coefficient can be neglected. A value of $D_{Fe^{3+}} = 1.812 \times 10^{-5}$ cm^2 s^{-1} at infinite dilution was used for iron(III) ions.[34] Assuming a quenching efficiency of 1 the effective particle radius is $R_{QD} \approx 4$ nm. After subtraction of the radius determined by TEM this equals a distance of 1.1 nm between the electron scavenger and the particle surface.

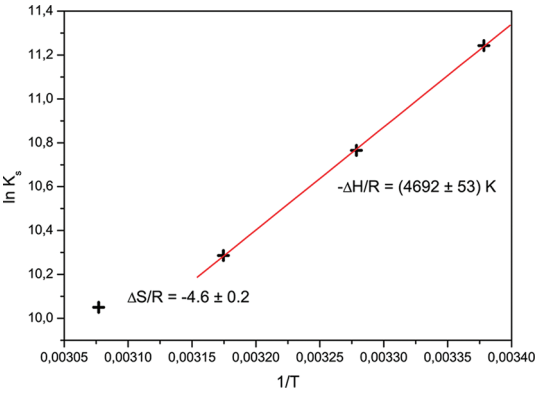

Figure 4. Temperature dependence of the Stern–Volmer constant of cysteine-capped QDs quenched statically by Fe^{3+} ions. Adsorption enthalpy and entropy were determined from the van't Hoff plot. The nonlinear behavior of the data at room temperature was attributed to the onset of photooxidation and particle aggregation during the measurement.

No quenching was observed with methyl viologen. It can be assumed that the quencher molecules do not come in close enough contact with the particle surface for the electron transfer to take place, while smaller metal ions pass that barrier or are accumulated in high enough concentrations to enable electron transfer. This has been attributed to an inner layer of the organic shell, which consists of densely packed ligands, while the outer part of the PEO chain has been swelled by the solvent. Diffusion of small molecules and ions is relatively unhindered in the outer ligand shell and comparable to free solution.

The diffusion model requires a number of assumptions: In reality the quenching efficiency is likely to be lower than 1. At very high iron concentrations the QD PL was found to saturate at 50–70% of the initial intensity. This corresponds to a quencher-particle distance of approximately 1.8 nm. Also, due to the swelled PEO layer the viscosity of the medium is likely to

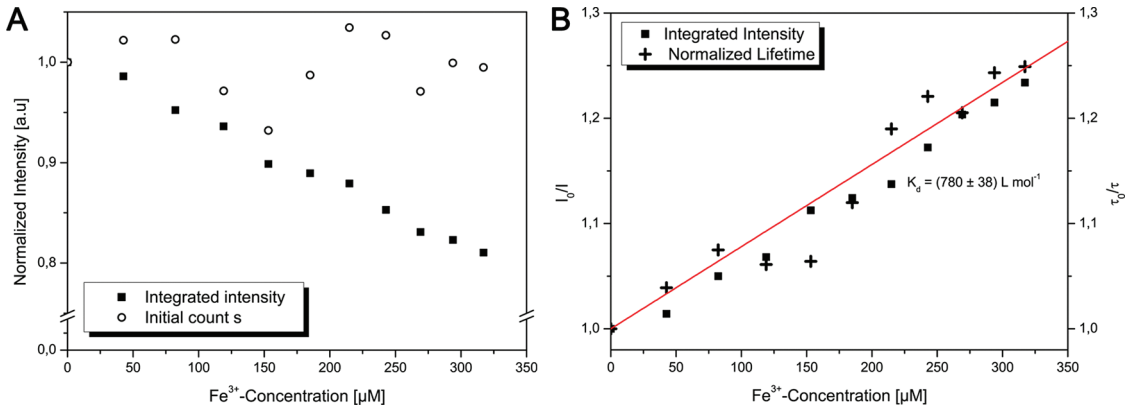

Figure 5. (A) Normalized fluorescence intensity (■) and initial counts of the fluorescence decay curve (○) of PEO(SH)$_3$-capped QDs plotted against Fe^{3+} concentration. (B) Stern−Volmer plot of the PL intensity and fluorescence lifetime (+). Linear regression yielded the Stern−Volmer constant K_d.

increase gradually near the particle surface. With a lower Fe^{3+} diffusion coefficient the thickness of the impenetrable inner layer shifts to larger values, limited by the electron tunneling mechanism, which does not occur over distances longer than a few angströms. An increased distance between quencher and particle surface indicates an accumulation of iron ions inside the PEO layer, which compensates the decrease in tunneling probability. Complexation of metal ions by PEO has been described previously in the literature.[37−39]

In acetate buffer solution at pH 5 the Stern−Volmer constant depended on the particle concentration, which was not observed at neutral pH. The relationship of K_d to the particle concentration was reciprocal (Figure 6). This behavior indicates a destabilization of the particle system that is independent of the actual quenching reaction. Since the surface ligands were in equilibrium at the beginning of the measurement, the decrease of K_d was attributed to desorption of protonated ligand molecules due to photooxidation and the dilution caused by the added quencher solution. This, in turn, increased the ligand shell's permeability for the quenching agent.

Energy Transfer. The fluorescence of cysteine- and PEO(SH)$_3$-capped QDs was quenched by adding an aqueous solution of BODIPY TR conjugated with a cadaverine moiety. The absorption of the fluorescent dye overlaps strongly with the PL spectrum of small CdSe/$Cd_xZn_{1-x}S$/ZnS QDs, while the emission spectra of the two species can be separated with optical filters (Figure 7A). BODIPY TR has minimal absorption at the employed excitation wavelength of 438 nm and an extinction coefficient of 64000 cm^{-1} M^{-1} at the absorption maximum of 588 nm, which is relatively independent of the solvent.[40] The PL QY was determined to be ~0.6 in water.

In FRET theory the distance between donor and acceptor fluorophor can be calculated from the Förster radius R_0, at which the transfer efficiency is exactly 0.5.[41]

$$R_0^6 = \frac{9(\ln 10)}{128\pi^5 N_A} \kappa^2 n^{-4} \Phi_0 J(\lambda) \quad (4)$$

R_0 depends on the relative dipole orientation factor κ^2, which is $^2/_3$ in isotropic distributions, the refractive index of the medium n, the quantum yield of the free donor Φ_0, and the overlap integral $J(\lambda)$ of the donor emission spectrum normalized to unit area and acceptor extinction coefficient as a measure of the dipole oscillator strengths.[42]

$$J(\lambda) = \int_0^\infty I_D(\lambda)\varepsilon_A(\lambda)\lambda^4 \, d\lambda \quad (5)$$

In isotropic solution, where donor and acceptor diffuse freely, the ratio of the donor intensity to the PL of free donor particles is given by

$$\frac{I_{DA}}{I_D} = 1 - \sqrt{\pi}\gamma \, e^{\gamma^2}(1 - \mathrm{erf}(\gamma)) \quad (6)$$

in which erf(x) is the error function. The acceptor concentration [A] is expressed by the dimensionless number γ.

$$\gamma = \frac{\sqrt{\pi}}{2} \frac{[A]}{[A]_0} \quad (7)$$

The distance dependence is introduced into the equation as the characteristic concentration $[A]_0$, which depends on R_0 and gives the concentration at which the energy transfer efficiency is 0.72.[43]

$$[A]_0 = \frac{1}{N_A}\left(\frac{4}{3}\pi R_0^3\right)^{-1} \quad (8)$$

The characteristic concentration for PEO(SH)$_3$- and cysteine-stabilized particles was calculated to be 458 and 1176 μM, respectively, with a numerical value for the overlap integral of 1.37×10^{-19} m^6 mol^{-1}. The difference between the two particle systems is due to their different quantum yields. Table 1 summarizes the calculated values. A diffractive index $n = 1.34$ of water at 434 nm was used.

The particles were titrated with a 0.83 μM BODIPY TR solution up to an acceptor concentration of 5 μM, well below the characteristic concentrations of both systems, and the spectra were corrected for the change

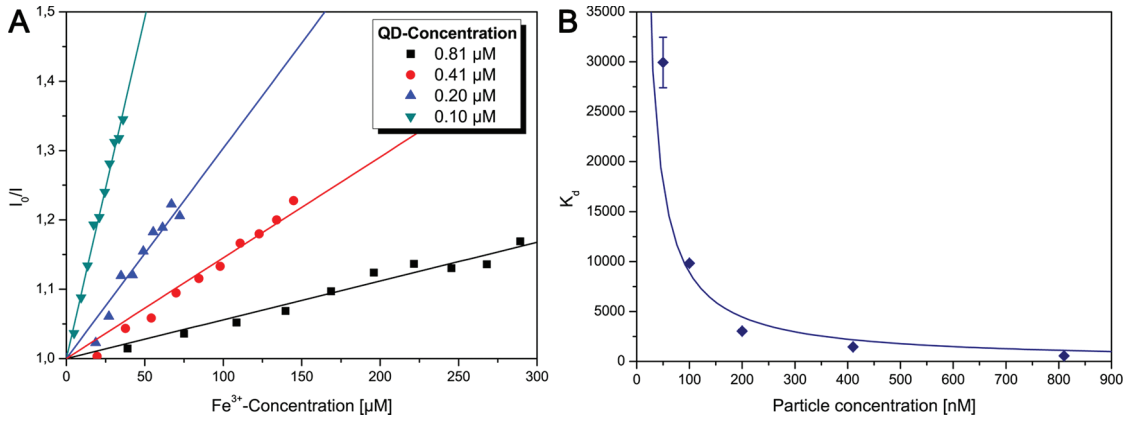

Figure 6. (A) Stern–Volmer plot of the PL intensity of $PEO(SH)_3$-capped QDs quenched with Fe^{3+} at pH 5. The quenching mechanism was dynamic. (B) The Stern–Volmer constant K_d as a function of particle concentration can be fitted to a reciprocal function. The error bars for the values at high particle concentration are too small to be displayed.

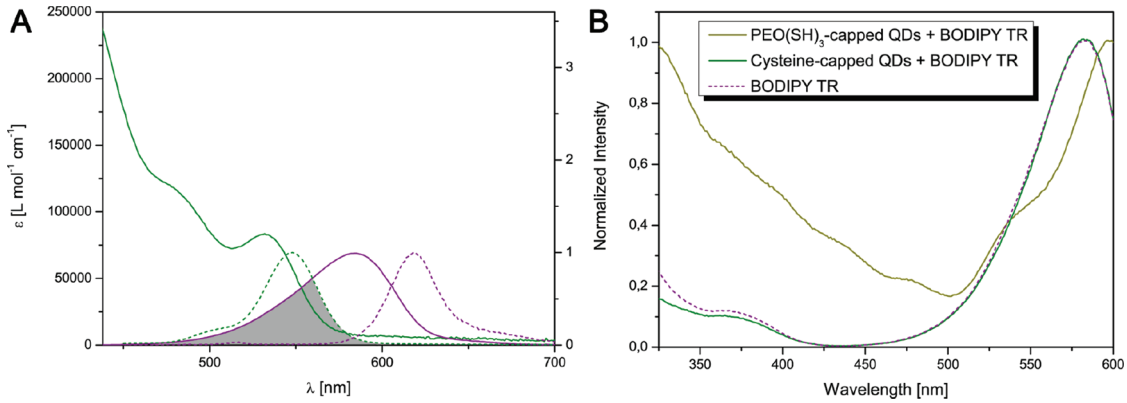

Figure 7. (A) Extinction coefficient (straight lines) and normalized PL spectra (dotted lines) of the employed particles (green) and BODIPY TR (violet). The overlap between donor emission and acceptor absorption is marked in gray. (B) Excitation spectra of QDs stabilized with cysteine (green) and $PEO(SH)_3$ (yellow) in the presence of BODIPY TR, as well as pure dye solution (violet). The spectra have been detected at an emission wavelength of 616 nm.

in volume. As can be expected cysteine-capped particles showed no FRET to dye molecules at this concentration. This can be observed in the excitation spectrum of a mixture of cysteine-capped particles and BODIPY TR, which was detected at the dye emission wavelength of 616 nm and is equal to that of pure dye molecules (Figure 7B). The occurrence of binding between the particle surface and the dye *via* the amine group of the cadaverine moiety can thus be excluded.

In contrary to the results from cysteine-capped QDs, the excitation spectrum of $PEO(SH)_3$-capped particles with BODIPY TR showed characteristic signals of the particle absorption spectrum, which indicates FRET between the fluorophores. The particles do not emit at the detection wavelength. A shift of the BODIPY TR peak in the excitation spectrum to larger wavelengths was attributed to the change in polarity that the dye molecules experience in proximity to PEO ligands. During the titration of the QDs with BODIPY TR the particle emission was significantly quenched to 20% of the original intensity at a dye concentration of 5 μM, which was accompanied by an increase in dye emission (Figure 8). A fit of eq 6 to the data resulted in a characteristic concentration of 3.3 μM. Comparing this value to the characteristic concentration calculated from eq 8 leads to a local dye concentration in the vicinity of the particles that is by a factor of 140 larger than for a homogeneous distribution. The reason for this is an accumulation of the dye inside the ligand shell, likely driven by the limited solubility of BODIPY TR in water and higher solubility in PEO.[44]

TABLE 1. Calculated Values for FRET between $PEO(SH)_3$- or Cysteine-Stabilized QDs

ligand	Φ_0	R_0 (nm)	$[A]_0$ (μM)
$PEO(SH)_3$	0.30	9.5	458
cysteine	0.05	7.1	1176

The volume V_{PEO} and radius of one particle with its PEO shell was calculated from the characteristic concentration by assuming a quantitative uptake of dye into the PEO and neglecting the inorganic QD volume due to the approximation of point dipoles in

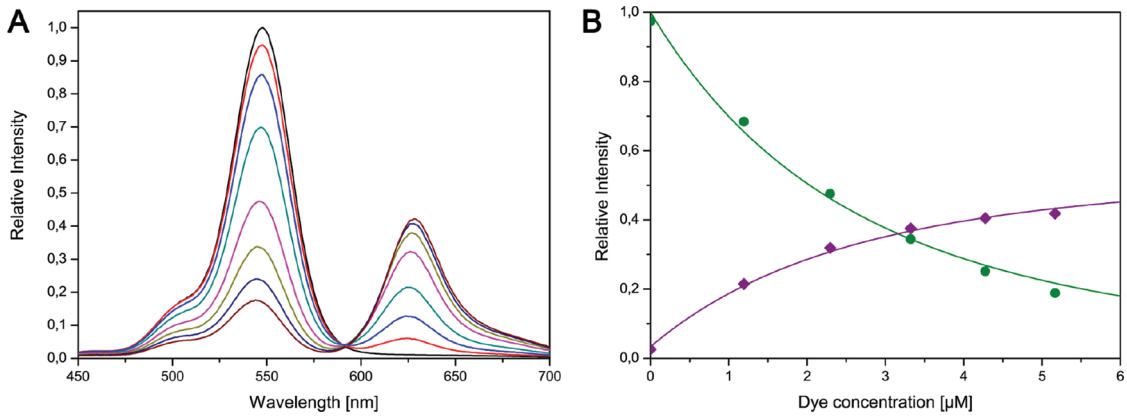

Figure 8. (A) PL Spectra of PEO(SH)$_3$-stabilized QDs after successive addition of aliquots of a BODIPY TR solution. (B) PL intensities of the particles (green) and the dye (violet) as a function of dye concentration.

Förster's theory. The total volume of all particles is equal to the number of dye molecules n_{dye} multiplied by the Förster volume $V_{Förster}$.

$$n_{QD}V_{PEO} = n_{dye}V_{Förster} = [A]_0 N_A \frac{4}{3}\pi R_0^3 \qquad (9)$$

This calculation yielded a volume of $V_{PEO} = 1.44 \times 10^4$ nm^3 and a particle radius of $r = 15.1$ nm. The particle concentration was determined from absorption spectra employing the empirical formula by Yu *et al.*[45] A discussion of the applicability of this method on core/shell particles can be found in the Supporting Information of a previous publication.[17] Assuming a factor of 2 as the maximal error for the QD concentration the particle radius lies in the interval between 12 and 19 nm with a tendency to smaller values. These values are in good agreement with the hydrodynamic radii of 10−15 nm determined by DLS.

The analysis of QD fluorescence decay curves showed that the particle fluorescence was statically quenched by the dye molecules. The initial photon count decreased by 20% after addition of 1equiv of BODIPY TR, while the fluorescence lifetime $\langle\tau_{QD}\rangle$ = 17.9 ns did not change significantly. The Stern−Volmer constant $K_s = 3.6 \times 10^5$ L mol^{-1} was 1 order of magnitude larger than the one for the adsorption of Fe^{3+} to cysteine-capped QDs. Funston *et al.* report complete, static quenching of hydrophobic QDs conjugated with Texas Red *via* a cadaverine bridge in agreement with these results.[46] Contrary to these reports we found no enhancement of the total emission intensity of the system with increasing dye concentration. The intensity was at 92% of the original value at a donor−acceptor ratio of 1:1 and decreased to 60% at a 6-fold excess of BODIPY TR. Extrapolation of the acceptor intensity to eq 6 showed a saturation at 51% of the initial donor intensity at high dye concentrations. The fluorescence lifetime of the dye was close to the experimentally determined value $\tau_{dye} = 5.2$ ns of free BODIPY TR at low concentrations and decreased exponentially to 60% with increasing concentration (Supporting Information, Figure S7). This behavior is explained by a locally high dye concentration inside the PEO shell. Homotransfer between dye molecules favors nonradiative deactivation and lowers the PL QY.

CONCLUSIONS

These results of the quenching experiments with PEO-capped semiconductor quantum dots allow a picture of the ligand shell's inner structure. It contains a densely packed inner shell of 1−2 nm that contains the ligand head groups and represents a barrier for small, organic molecules and to a lesser extent for metal ions. The outer shell of swelled polymer is less densely packed and allows small molecules to diffuse freely. BODIPY TR molecules, which function as acceptors for Förster resonance energy transfer, are accumulated in the PEO shell and effectively quench the particle fluorescence. The PEO shell's volume was calculated from the quenching efficiency using a model of freely diffusing acceptor molecules. The effective particle radius could be estimated to be 12 nm, which is in good agreement with the measured hydrodynamic radius.

EXPERIMENTAL SECTION

Materials. Milli-Q water (Millipore) was used as bidistilled water. All solvents were of analytical grade and purchased from Merck or Th. Geyer GmbH. *n*-Trioctylphosphine (TOP), *n*-trioctylphosphine oxide (TOPO), L-cysteine, *N*-ethyldiisopropyl amine, and methyl viologen dichlorid were purchased from Sigma-Aldrich, hexadecyl amine (HDA), iron(III) nitrate nonahydrate and zinc acetate dihydrate from Merck, selenium and *n*-tetradecyl phosphonic acid (TDPA) from Alfa Aesar, pentaerythritol tetrakis(3-mercaptopopionate) from Fluka, anhydrous cadmium acetate from ChemPur, and poly(ethylene oxide) monoacrylate from Monomer-Polymer & Dajac

Laboratories, Inc. BODIPY TR cadaverine was purchased from Invitrogen.

Characterization. Absorption spectra were acquired with a Cary 50 UV−vis spectrometer (Varian); PL spectra were acquired with a Fluorolog-3 and Fluoromax-4 spectrometer (Horiba Jobin Yvon). Time-resolved single photon counting was performed with a PDL 800-D pulsed diode laser at a wavelength of 438 nm and detected with a PMA-M 185 photomultipier with a resolution of 250 ps (PicoQuant). The signal was processed by a constant-fraction 200 MHz discriminator and a time-to-amplitude converter (EG&G Ortec). Curve fitting was performed with the software FluoFit 4.4 (PicoQuant). DLS measurements were performed with a Zetasizer Nano ZS ZEN 3600 (Malvern Instruments).

Particle Synthesis. The core/shell/shell nanoparticles were synthesized following published protocols.[5,7] Briefly, cadmium acetate dissolved in TOP was rapidly injected into a mixture of TOPO, HDA, TDPA, and selenium in TOP at 300 °C. The temperature was lowered to 260 °C and the particles were allowed to grow to the desired size. Toluene was added after cooling to room temperature, and the product was cleaned by precipitating it three times with methanol and dissolving in chloroform.

The shells were synthesized by adding freshly prepared CdSe into a mixture of TOPO, HDA and TDPA. For the first shell, a solution of cadmium and zinc acetate in TOP was injected at 200 °C, and H_2S gas was slowly added over the vigorously stirred solution with a syringe pump. A solution of zinc acetate in TOP was used for the second shell.

Synthesis of PEO(SH)$_3$. The PEO ligand was synthesized following the protocol of Thiry *et al.*[17] Briefly, poly(ethylene oxide) monoacrylate with the desired chain length was dissolved in chloroform and pentaerythritol tetrakis(3-mercaptopopionate) and *N*-ethyldiisopropyl amine were added. The solution was stirred for 72 h at 50 °C and precipitated with cold diethyl ether.

Ligand Exchange with PEO(SH)$_3$. Ligand exchange with PEO(SH)$_3$ was performed following the protocol of Thiry *et al.*[17] by precomplexating the ligands with zinc acetate in TOP and stirring the CdSe/Cd$_x$Zn$_{1-x}$S/ZnS particles in chloroform in the presence of an 4500-fold excess of ligand for 4 h. The particles were precipitated twice with hexane and dissolved in bidistilled water, dialyzed in a Vivaspin centrifugal unit with a MWCO of 10 kD and passed through a 0.2 mm CME syringe filter.

Ligand Exchange with Cysteine. Ligand exchange with L-cysteine was performed following the protocol of Liu *et al.*[10] by adding cysteine in bidistilled water to a solution of CdSe/Cd$_x$Zn$_{1-x}$S/ZnS particles in chloroform and stirring the biphasic mixture until the QDs had transferred into the aqueous solution. The particles were precipitated with ethanol and passed through a 0.2 μm CME syringe filter.

Sample Preparation and Analysis. The measurements were performed in quartz cuvettes filled with a volume of 2500 mL of a QD solution in water. The samples were allowed to equilibrate for 2 h in the dark. For the quenching series aliquots of the quencher solution (up to 1000 mL) were added, and fluorescence decay curves (TCSPC) and steady-state fluorescence spectra were acquired. The PL intensity was corrected for the dilution due to the added volume. In the case of Fe^{3+}, which absorbed at the excitation wavelength λ_{ex} = 438 nm, the inner filter effect for the excitation was also taken into account using Lakowicz's correction method.[47]

$$I_{corr} = \frac{I}{I_0}\frac{V}{V_0}10^{0.5\varepsilon_{Fe^{3+}}(\lambda_{ex})[Fe^{3+}]} \quad (10)$$

Iron nitrate solutions were freshly prepared before the experiment and aged for 3 h until the optical density remained constant.

Fluorescence decay curves from the time-resolved particle spectra were fitted with a stretched biexponential function.

$$I(t) = A_1\, e^{-(t/\tau_1)^{\beta_1}} + A_2\, e^{-(t/\tau_2)^{\beta_2}} \quad (11)$$

The stretching factor for the second decay component was set to $\beta_2 = 1$ to reduce the number of fitting parameters. The resulting monoexponential decay had a long fluorescence lifetime τ_2 in the order of several 100 ns and contributed less than 1% to the total decay. τ_2 was determined for free QDs and set constant in successive measurements. Schöps *et al.* have reported similar behavior for CdTe/CdS particles, which they contributed to the decay of dark excitons, trap emission or charge separation.[48] The mean lifetime of the particles was calculated as

$$\langle\tau\rangle = \frac{\tau_1}{\beta_1}\Gamma\left(\frac{1}{\beta_1}\right) \quad (12)$$

where $\Gamma(x)$ is the Gamma function.[49] The stretching factor β_1 is a measure for the distribution within the particle sample. It correlated with the initial PL QY of the particles and varied between 0.9 for high and 0.4 for low quantum yields. No significant trend for β_1 was observed during the course of one measurement; the sample homogeneity of the particle ensemble was therefore assumed to be unchanged.[50]

Acknowledgment. The authors would like to thank S. Bartholdy-Nawrath for TEM micrographs. Funding was provided by the state excellence initiative Nanotechnology in Medicine (BMBF).

Supporting Information Available: Fluorescence decay curves of cysteine-capped QDs quenched with MV^{2+}, discussion of single particle time traces of PEO(SH)$_3$-capped nanocrystals with and without Fe^{3+}, fluorescence lifetimes of BODIPY TR inside PEO ligand shells as a function of dye concentration. This material is available free of charge *via* the Internet at http://pubs.acs.org.

REFERENCES AND NOTES

1. Michalet, X.; Pinaud, F.; Bentolila, L.; Tsay, J.; Doose, S.; Li, J. J.; Sundaresan, G.; Wu, A.; Gambhir, S.; Weiss, S. Quantum Dots for Live Cells, *in Vivo* Imaging, and Diagnostics. *Science* **2005**, *307*, 538–544.
2. Somers, R. C.; Bawendi, M. G.; Nocera, D. G. CdSe Nanocrystal Based Chem-/Bio- Sensors. *Chem. Soc. Rev.* **2007**, *36*, 579.
3. Niemeyer, C. M. Nanoparticles, Proteins, and Nucleic Acids: Biotechnology Meets Materials Science. *Angew. Chem., Int. Ed.* **2001**, *40*, 4128–4158.
4. Murray, C. B.; Norris, D. J.; Bawendi, M. G. Synthesis and Characterization of Nearly Monodisperse CdE (E = S, Se, Te) Semiconductor Nanocrystallites. *J. Am. Chem. Soc.* **1993**, *115*, 8706–8715.
5. Mekis, I.; Talapin, D. V.; Kornowski, A.; Haase, M.; Weller, H. One-Pot Synthesis of Highly Luminescent CdSe/CdS Core−Shell Nanocrystals *via* Organometallic and "Greener" Chemical Approaches. *J. Phys. Chem. B* **2007**, *107*, 7454–7462.
6. Peng, X. An Essay on Synthetic Chemistry of Colloidal Nanocrystals. *Nano Res.* **2009**, *2*, 425–447.
7. Talapin, D. V.; Mekis, I.; Götzinger, S.; Kornowski, A.; Benson, O.; Weller, H. CdSe/CdS/ZnS and CdSe/ZnSe/ZnS Core−Shell−Shell Nanocrystals. *J. Phys. Chem. B* **2006**, *108*, 18826–18831.
8. Nikolić, M. S.; Krack, M.; Aleksandrovic, V.; Kornowski, A.; Förster, S.; Weller, H. Tailor-Made Ligands for Biocompatible Nanoparticles. *Angew. Chem., Int. Ed.* **2006**, *45*, 6577–6580.
9. Stewart, M.; Susumu, K.; Mei, B.; Medintz, I.; Delehanty, J.; Blanco-Canosa, J.; Dawson, P.; Mattoussi, H. Multidentate Poly(ethylene glycol) Ligands Provide Colloidal Stability to Semiconductor and Metallic Nanocrystals in Extreme Conditions. *J. Am. Chem. Soc.* **2010**, *132*, 9804–9813.
10. Liu, W.; Choi, H.; Zimmer, J.; Tanaka, E.; Frangioni, J.; Bawendi, M. Compact Cysteine-Coated CdSe (ZnCdS) Quantum Dots for *in Vivo* Applications. *J. Am. Chem. Soc.* **2007**, *129*, 14530–14531.
11. Pöselt, E.; Fischer, S.; Foerster, S.; Weller, H. Highly Stable Biocompatible Inorganic Nanoparticles by Self-Assembly of Triblock-Copolymer Ligands. *Langmuir* **2009**, *25*, 13906–13913.
12. Pellegrino, T.; Manna, L.; Kudera, S.; Liedl, T.; Koktysh, D.; Rogach, A. L.; Keller, S.; Rädler, J.; Natile, G.; Parak, W. J. Hydrophobic Nanocrystals Coated with an Amphiphilic Polymer Shell: A General Route to Water Soluble Nanocrystals. *Nano Lett.* **2007**, *4*, 703–707.

13. Tromsdorf, U. I.; Bigall, N. C.; Kaul, M. G.; Bruns, O. T.; Nikolić, M. S.; Mollwitz, B.; Sperling, R. A.; Reimer, R.; Hohenberg, H.; Parak, W. J.; *et al*. Size and Surface Effects on the MRI Relaxivity of Manganese Ferrite Nanoparticle Contrast Agents. *Nano Lett.* **2007**, *7*, 2422–2427.
14. Uyeda, H. T.; Medintz, I. L.; Jaiswal, J. K.; Simon, S. M.; Mattoussi, H. Synthesis of Compact Multidentate Ligands to Prepare Stable Hydrophilic Quantum Dot Fluorophores. *J. Am. Chem. Soc.* **2010**, *127*, 3870–3878.
15. Soo Choi, H.; Liu, W.; Misra, P.; Tanaka, E.; Zimmer, J. P.; Itty Ipe, B.; Bawendi, M. G.; Frangioni, J. V. Renal Clearance of Quantum Dots. *Nat. Biotechnol.* **2007**, *25*, 1165–1170.
16. Harris, J. M., Ed. *Poly(Ethylene Glycol) Chemistry: Biotechnical and Biomedical Application*, 1st ed.; Springer: Berlin, 1992.
17. Thiry, M.; Boldt, K.; Nikolić, M. S.; Schulz, F.; Ijeh, M.; Panicker, A.; Vossmeyer, T.; Weller, H. Fluorescence Properties of Hydrophilic Semiconductor Nanoparticles with Tridentate Polyethylene Oxide Ligands. *ACS Nano* **2011**, *5*, 4965–4973.
18. Kirchner, C.; Liedl, T.; Kudera, S.; Pellegrino, T.; Javier, A. M.; Gaub, H. E.; Stölzle, S.; Fertig, N.; Parak, W. J. Cytotoxicity of Colloidal CdSe and CdSe/ZnS Nanoparticles. *Nano Lett.* **2004**, *5*, 331–338.
19. Yildiz, I.; Tomasulo, M.; Raymo, F. Electron and Energy Transfer Mechanisms to Switch the Luminescence of Semiconductor Quantum Dots. *J. Mater. Chem.* **2008**, *18*, 5577–5584.
20. Cui, S.-C.; Tachikawa, T.; Fujitsuka, M.; Majima, T. Solvent-Polarity Dependence of Electron-Transfer Kinetics in a CdSe/ZnS Quantum Dot-Pyromellitimide Conjugate. *J. Phys. Chem. C* **2010**, *114*, 1217–1225.
21. Scholes, G. D. Long-Range Resonance Energy Transfer In Molecular Systems. *Annu. Rev. Phys. Chem.* **2003**, *54*, 57–87.
22. Medintz, I. L.; Uyeda, H. T.; Goldman, E. R.; Mattoussi, H. Quantum Dot Bioconjugates for Imaging, Labelling and Sensing. *Nat. Mater.* **2005**, *4*, 435–447.
23. Medintz, I.; Mattoussi, H. Quantum Dot-Based Resonance Energy Transfer and its Growing Application in Biology. *Phys. Chem. Chem. Phys.* **2009**, *11*, 17–45.
24. Baer, R.; Rabani, E. Theory of Resonance Energy Transfer Involving Nanocrystals: The Role of High Multipoles. *J. Chem. Phys.* **2008**, *128*, 184710.
25. Förster, T. Zwischenmolekulare Energiewanderung und Fluoreszenz (Intermolecular Energy Migration and Fluorescence). *Ann. Phys.* **1948**, *6*, 55–75.
26. Allan, G.; Delerue, C. Energy Transfer Between Semiconductor Nanocrystals: Validity of Förster's Theory. *Phys. Rev. B* **2007**, *75*, 195311.
27. Rogach, A. L.; Klar, T. A.; Lupton, J. M.; Meijerink, A.; Feldmann, J. Energy Transfer with Semiconductor Nanocrystals. *J. Mater. Chem.* **2009**, *19*, 1208.
28. Soujon, D.; Becker, K.; Rogach, A. L.; Feldmann, J.; Weller, H.; Talapin, D. V.; Lupton, J. M. Time-Resolved Förster Energy Transfer from Individual Semiconductor Nanoantennae to Single Dye Molecules. *J. Phys. Chem. C* **2008**, *111*, 11511–11515.
29. Franzl, T.; Klar, T. A.; Schietinger, S.; Rogach, A. L.; Feldmann, J. Exciton Recycling in Graded Gap Nanocrystal Structures. *Nano Lett.* **2004**, *4*, 1599–1603.
30. Potapova, I.; Mruk, R.; Hübner, C.; Zentel, R.; Basché, T.; Mews, A. CdSe/ZnS Nanocrystals with Dye-Functionalized Polymer Ligands Containing Many Anchor Groups. *Angew. Chem., Int. Ed.* **2005**, *44*, 2437–2440.
31. Weller, H.; Koch, U.; Gutiérrez, M.; Henglein, A. Photochemistry of Colloidal Metal Sulfides. 7. Absorption and Fluorescence of Extremely Small ZnS Particles (The World of the Neglected Dimensions). *Ber. Bunsen. Phys. Chem.* **1984**, *88*, 649–656.
32. Hässelbarth, A.; Eychmüller, A.; Weller, H. Detection of Shallow Electron Traps in Quantum Sized CdS by Fluorescence Quenching Experiments. *Chem. Phys. Lett.* **1993**, *203*, 271–276.
33. Watanabe, T.; Honda, K. Measurement of the Extinction Coefficient of the Methyl Viologen Cation Radical and the Efficiency of Its Formation by Semiconductor Photocatalysis. *J. Phys. Chem.* **2001**, *86*, 2617–2619.
34. Lide, D. R., Ed. *Handbook of Chemistry and Physics*, 79th ed.; CRC Press: Boca Raton, 1998.
35. Ding, L.; Zhou, P. J.; Li, S. Q.; Shi, G. Y.; Zhong, T.; Wu, M. Spectroscopic Studies on the Thermodynamics of L-Cysteine Capped CdSe/CdS Quantum Dots—BSA Interactions. *J. Fluoresc.* **2010**, *21*, 17–24.
36. Dohmen, M. P. J.; Pereira, A. M.; Timmer, J. M. K.; Benes, N. E.; Keurentjes, J. T. F. Hydrodynamic Radii of Polyethylene Glycols in Different Solvents Determined from Viscosity Measurements. *J. Chem. Eng. Data* **2008**, *53*, 63–65.
37. Lamb, J. D.; Nazarenko, A. Y.; Neilson, L. Novel Extraction of Metal Ions from Acidic Media Using Poly(ethylene oxide) Phases. *Anal. Commun.* **1998**, *35*, 145–146.
38. Uekawa, N.; Endo, M.; Kakegawa, K.; Sasaki, Y. Homogeneous Precipitation of Cr^{3+}–M^{2+} (M = Ni, Zn, Co, Cu) Oxalate by Oxidation of the Polyethylene Clycol–Cation Complex. *Phys. Chem. Chem. Phys.* **2000**, *2*, 5485–5490.
39. Xie, K.; Huang, K.; Xu, L.; Yu, P.; Yang, L.; Liu, H. Three-Liquid-Phase Extraction and Separation of Ti(IV), Fe(III), and Mg(II). *Ind. Eng. Chem. Res.* **2011**, *50*, 6362–6368.
40. Johnson, I., Spence, M. T. Z., Eds. *The Handbook: A Guide to Fluorescent Probes and Labeling Technologies*, 11th ed.; Molecular Probes: Eugene, OR, 2010.
41. An expression for R_0^6 is often given in the literature that differs from the one presented here by a factor of 1000. Owing to the dependency on the sixth power of R_0 this is not a simple scaling factor. The equation used in this publication has been verified by the authors for wavelengths given in nm, the extinction coefficient in $cm^{-1}\ M^{-1}$ and a factor of $10^{-37} m^6\ mol^{-1}$ resulting from conversion to SI units.
42. Förster, T. Transfer Mechanisms of Electronic Excitation. *Discuss. Faraday Soc.* **1959**, *27*, 7–17.
43. Förster, T. Experimentelle und Theoretische Untersuchung des Zwischenmolekularen Ubergangs von Elektronenanregungsenergie (Experimental and Theoretical Investigation of the Transition from Intermediate Molecular Electron Excitation Energy). *Z. Naturforsch.* **1949**, *4a*, 321–327.
44. Lavis, L. D.; Raines, R. T. Bright Ideas for Chemical Biology. *ACS Chem. Biol.* **2008**, *3*, 142–155.
45. Yu, W. W.; Qu, L.; Guo, W.; Peng, X. Experimental Determination of the Extinction Coefficient of CdTe, CdSe, and CdS Nanocrystals. *Chem. Mater.* **2005**, *15*, 2854–2860.
46. Funston, A. M.; Jasieniak, J. J.; Mulvaney, P. Complete Quenching of CdSe Nanocrystal Photoluminescence by Single Dye Molecules. *Adv. Mater.* **2008**, *20*, 4274–4280.
47. Lakowicz, J. R. *Principles of Fluorescence Spectroscopy*, 3rd ed.; Springer: New York, 2010.
48. Schöps, O.; Thomas, N. L.; Woggon, U.; Artemyev, M. Recombination Dynamics of CdTe/CdS Core–Shell Nanocrystals. *J. Phys. Chem. B* **2007**, *110*, 2074–2079.
49. Schlegel, G.; Bohnenberger, J.; Potapova, I.; Mews, A. Fluorescence Decay Time of Single Semiconductor Nanocrystals. *Phys. Rev. Lett.* **2002**, *88*, 137401.
50. Lindsey, C. P.; Patterson, G. D. Detailed comparison of the Williams–Watts and Cole–Davidson functions. *J. Chem. Phys.* **2002**, *73*, 3348–3357.